ELECTROMAGNETIC SUSCEPTIBILITY MODEL OF DISCONTINUOUS MICROSTRIP CIRCUITS UNDER PLANE WAVE ILLUMINATION

S. R. Li, Y. Li*, Z. Sun, and F. Wang

School of Electrical and Electronic Engineering, North China Electric Power University, Beijing 102206, China

Abstract—The electromagnetic susceptibility model of discontinuous microstrip circuits with the presence of a uniform plane incident wave is established. First, the analytical expressions are modeled as equivalent voltage and current sources for discussing the global effect of the incident plane wave on the associated interconnects. Then, these field-induced equivalent source expressions are incorporated into ADS circuit solver, and a fast model is established for analyzing the output responses of discontinuous microstrip circuits, such as the cross bend, the band-rejection filter and the single-stage amplifier. The corresponding simulation results from the proposed model are validated by comparing the results from both simulation and measurement. The results also show that the incident plane wave may influence the output terminal responses significantly, and the proposed approach would be an efficient method to solve the electromagnetic susceptibility problems associated with the discontinuous microstrip circuits.

1. INTRODUCTION

With the rapid development of electronic technology, modern electronic equipments have been widely used in various fields, which increase the complexity of electromagnetic (EM) environment around us. The unwanted electromagnetic environment pollution has emerged, resulting in the electromagnetic compatibility problems [l–3]. Integration and high speed of electronic devices contribute to the transmission line effects of the microstrip interconnect on the printed circuit board (PCB). The interconnect, which functions as

an antenna or a transmission line, will increase the electromagnetic interference (EMI) susceptibility and radiation efficiency of the conducting traces [4, 5]. So careful modeling strategies of modern electronic systems during early design stages are required, otherwise these EMI effects may cause the system failures.

An external EM plane wave field coupled into the circuit on a PCB is mainly through the trace interconnects. In the past research work, there are two mainstream approaches to analyze the related EMI problems of circuits. One is based on the transmission line coupling theory and the second one is based on full-wave methods.

Generally speaking, the field-coupled problem of interconnects has been discussed in [6–8]. The simplified coupling case that is illuminated by a plane EM wave is considered in [9, 10], and an approximate analytical expression based on transmission line theory has been provided. In addition, the EMI problems associated with high-speed interconnects have also been studied in [11, 12]. Essentially, most of the techniques dealing with field-coupled problems are based on the formulation presented by Taylor [13]. However, interconnect discontinuities which are usually analyzed by this approach can lead to significant failures due to their inability to account for higher order modes.

These difficulties can be discussed using full-wave characterization of EM modules. Voltages and currents induced at the terminal of the circuit by coupling of electromagnetic waves are obtained from the solution of the field quantities directly. With its advantages of simple algorithm and readily broadband analysis ability, the FDTD method is a good candidate among all the full-wave approaches [14–17]. FDTD method has been widely used to analyze interconnect structures especially in the solution of planar microwave circuits in the last two decades [18–20]. In FDTD, the lumped components are modeled as grid or sub-grid elements. However, the stiff differential equations representing networks with linear/nonlinear lumped circuit components require step size far below Courant condition, leading to impractical CPU times, and then the explicit integration scheme turns into a handicap in circuit applications from the numerical stability point of view, which works to the advantage of FDTD in field analysis.

Up to now, it seems that few papers were reported to quickly handle the EMI problems associated with the microstrip circuits which include interconnect discontinuities. In this paper, a hybrid method based on equations and the circuit solver is proposed to discuss the electromagnetic susceptibility of the discontinuous microstrip circuits, such as the cross bend, the band-rejection filter and the single-stage amplifier. We show the results of the time domain voltages and the

alternating voltages in the terminal of these discontinuous microstrip circuits, and they are compared to the measurement results and simulation results from other papers.

2. EQUIVALENT CIRCUIT FOR MICROSTRIP ELEMENTS

Basically, it is difficult to precisely analyze field-influenced responses of the microstrip circuit, which is illuminated by a uniform incident plane wave, due to the complexity of the microstrip circuit on a PCB. A microstrip circuit mainly includes lumped elements (chipset resistors/capacitors), active components, and microstrip line traces. The microstrip line elements contribute all field-induced equivalent sources for the microstrip circuit on a PCB. Thus, the microstrip circuit will be modeled as a cascade of several microstrip elements.

The microstrip cross bend shown in Fig. 1 will be addressed in this section, and then other typical discontinuous microstrip elements, such as a right-angle bend, a T-type bend will be easily discussed. Here, the associated conductors for this cross-bend structure are assumed to be perfect, and the strip width w and thickness t are much smaller than the wavelength. It is also assumed that the substrate with relative permittivity ε_r and thickness h is lossless.

The cross-bend junction is modeled as the lumped-element (L, C) equivalent circuit in Fig. 1(b). The method of calculating values of capacitance C and inductance L for the equivalent circuit is given in [21]. This cross-bend junction is connected to the loads Z_{L1}, Z_{L2}, Z_{L3} and Z_{L4}, at (x_1, y_1), (x_2, y_2), (x_3, y_3) and (x_4, y_4), respectively. Being illuminated by the incident wave field $\vec{E}^{inc}$, there would be some distributed voltage and current induced along each microstrip arm (such as the a-arm) so that their global effect may be represented by the total field-induced equivalent voltage and current sources, (V_a, I_a) at the line terminal, as shown in Fig. 1(c). By the same mechanism, similar field-induced equivalent sources (V_b, I_b), (V_c, I_c) and (V_d, I_d) will be presented at the terminals of the b-, c-, and d-arms, respectively. Here (Z_{oa}, β_a), (Z_{ob}, β_b), (Z_{oc}, β_c) and (Z_{od}, β_d) are the characteristic impedances and phase constants of the a-, b-, c-, and d-arms, respectively.

As shown in Fig. 2, an incident plane wave is determined by the angles of incidence θ and ϕ (Fig. 2(a)). The polarization of the wave is defined by the angle γ (Fig. 2(b)). Specifically, the incident plane

(a)

(b)

(c)
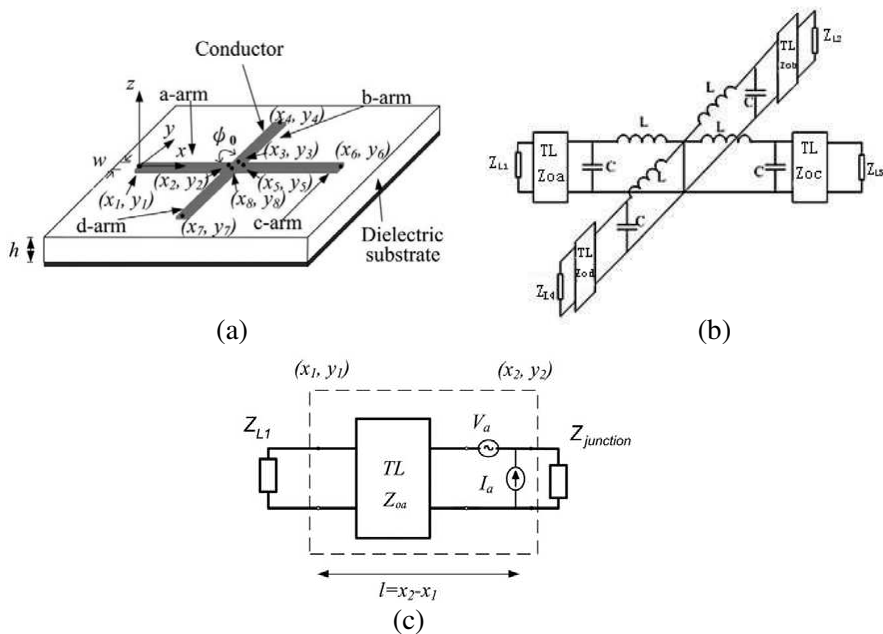
Figure 1. Microstrip cross-bend structure. (a) Geometry, (b) equivalent lumped element representation of the cross-bend junction, (c) equivalent circuit model with field-induced voltage and current sources.

(a)

(b)
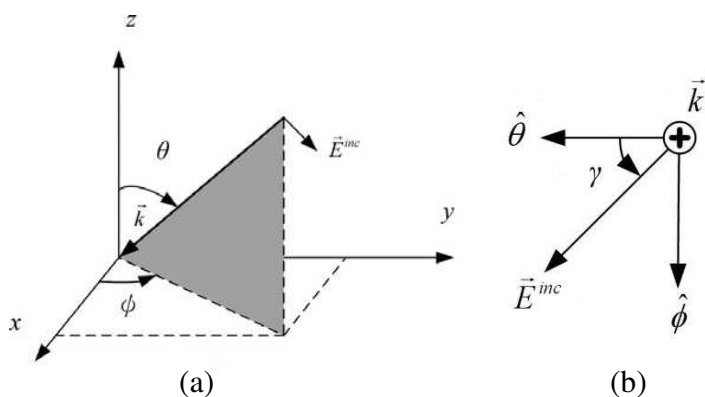
Figure 2. Parameters to characterize the incident plane wave. (a) Incidence angles (θ, ϕ), (b) polarization angle γ.

wave is expressed as follows:

$$\vec{E}^{inc} = E_0[(\cos\gamma\cos\theta\cos\phi - \sin\gamma\sin\phi)\hat{x} + (\cos\gamma\cos\theta\sin\phi + \sin\gamma\cos\phi)\hat{y}$$
$$- (\cos\gamma\sin\phi)\hat{z}]e^{-j(k_x x + k_y y + k_z z)}, \tag{1}$$

The components of phase constant, $(k_x,\ k_y,\ k_z)$, along the coordinate axes are as follows:

$$k_x = -k_0\sin\theta\cos\phi, \tag{2}$$
$$k_y = -k_0\sin\theta\sin\phi, \tag{3}$$
$$k_z = -k_0\cos\theta, \tag{4}$$
$$k_0 = \sqrt{\mu_0\varepsilon_0}. \tag{5}$$

Based on the field-line coupling theory in [22, 23], the field-induced equivalent sources $(V_a,\ I_a)$ or $(V_b,\ I_b)$ at the terminal of a- or b-arms may be expressed as follows:

$$V_a = \frac{1}{2}E_0 f_x e^{j\beta_a l_1}\left(\frac{1 - e^{-j(\beta_a + k_x)l_1}}{j(\beta_a + k_x)}\right)e^{-jk_x x_1}$$

$$+ \frac{1}{2}E_0 f_x e^{j\beta_a l_1}e^{-j\beta_a l_1}\left(\frac{e^{j(\beta_a - k_x)l_1} - 1}{j(\beta_a - k_x)}\right)e^{-jk_x x_1}$$

$$+ E_0 f_z\left(\frac{1 - e^{-jk_{2z}2h}}{jk_{2z}}\right)\left(\cos(\beta_a l_1) - e^{-jk_x l_1}\right)e^{-jk_x x_1}, \tag{6a}$$

$$I_a = -\frac{1}{2Z_{oa}}E_0 f_x e^{j\beta_a l_1}\left(\frac{1 - e^{-j(\beta_a + k_x)l_1}}{j(\beta_a + k_x)}\right)e^{-jk_x x_1}$$

$$+ \frac{1}{2Z_{oa}}E_0 f_x e^{j\beta_a l_1}e^{-j\beta_a l_1}\left(\frac{e^{j(\beta_a - k_x)l_1} - 1}{j(\beta_a - k_x)}\right)e^{-jk_x x_1}$$

$$- j\frac{1}{Z_{oa}}E_0 f_z\left(\frac{1 - e^{-jk_{2z}2h}}{jk_{2z}}\right)\sin(\beta_a l_1)e^{-jk_x x_1}, \tag{6b}$$

$$V_b = \frac{1}{2}E_0 f_y\left(e^{j\beta_b d_1}\left(\frac{1 - e^{-j(\beta_b + k_y)d_1}}{j(\beta_b + k_y)}\right)\right)e^{-jk_y y_3}$$

$$+ \frac{1}{2}E_0 f_y\left(e^{-j\beta_b d_1}\left(\frac{e^{j(\beta_b - k_y)d_1} - 1}{j(\beta_b - k_y)}\right)\right)e^{-jk_y y_3}$$

$$+ E_0 f_z\left(\frac{1 - e^{-jk_{2z}2h}}{jk_{2z}}\right)\left[\cos(\beta_b d_1) - e^{-jk_y d_1}\right]e^{-jk_y y_3}, \tag{7a}$$

$$
\begin{aligned}
I_b &= -\frac{1}{2Z_{ob}} E_0 f_y \left(e^{j\beta_b d_1} \left(\frac{1 - e^{-j(\beta_b + k_y)d_1}}{j(\beta_b + k_y)} \right) \right) e^{-jk_y y_3} \\
&\quad + \frac{1}{2Z_{ob}} E_0 f_y \left(e^{-j\beta_b d_1} \left(\frac{e^{j(\beta_b - k_y)d_1} - 1}{j(\beta_b - k_y)} \right) \right) e^{-jk_y y_3} \\
&\quad - j\frac{1}{Z_{ob}} E_0 f_z \left(\frac{1 - e^{-jk_{2z}2h}}{jk_{2z}} \right) \sin(\beta_b d_1) e^{-jk_y y_3},
\end{aligned}
\tag{7b}
$$

where $l_1 = x_2 - x_1$, $d_1 = y_4 - y_3$, and

$$
k_{2z} = k_0 \sqrt{\varepsilon_r - \sin^2 \theta}, \tag{8}
$$

$$
\begin{aligned}
f_x &= \cos\gamma \cos\theta \cos\phi - \cos\gamma \cos\theta \cos\phi \left(\frac{\left(\frac{\varepsilon_r \cos\theta - \sqrt{\varepsilon_r - \sin^2\theta}}{\varepsilon_r \cos\theta + \sqrt{\varepsilon_r - \sin^2\theta}} \right) + e^{-jk_{2z}2h}}{1 + \left(\frac{\varepsilon_r \cos\theta - \sqrt{\varepsilon_r - \sin^2\theta}}{\varepsilon_r \cos\theta + \sqrt{\varepsilon_r - \sin^2\theta}} \right) e^{-jk_{2z}2h}} \right) \\
&\quad - \sin\gamma \sin\phi \left(1 + \left(\frac{\left(\frac{\cos\theta - \sqrt{\varepsilon_r - \sin^2\theta}}{\cos\theta + \sqrt{\varepsilon_r - \sin^2\theta}} \right) - e^{-jk_{2z}2h}}{1 - \left(\frac{\cos\theta - \sqrt{\varepsilon_r - \sin^2\theta}}{\cos\theta + \sqrt{\varepsilon_r - \sin^2\theta}} \right) e^{-jk_{2z}2h}} \right) \right),
\end{aligned}
\tag{9}
$$

$$
\begin{aligned}
f_y &= \cos\gamma \cos\theta \sin\phi - \cos\gamma \cos\theta \sin\phi \left(\frac{\left(\frac{\varepsilon_r \cos\theta - \sqrt{\varepsilon_r - \sin^2\theta}}{\varepsilon_r \cos\theta + \sqrt{\varepsilon_r - \sin^2\theta}} \right) + e^{-jk_{2z}2h}}{1 + \left(\frac{\varepsilon_r \cos\theta - \sqrt{\varepsilon_r - \sin^2\theta}}{\varepsilon_r \cos\theta + \sqrt{\varepsilon_r - \sin^2\theta}} \right) e^{-jk_{2z}2h}} \right) \\
&\quad + \sin\gamma \cos\phi \left(1 + \left(\frac{\left(\frac{\cos\theta - \sqrt{\varepsilon_r - \sin^2\theta}}{\cos\theta + \sqrt{\varepsilon_r - \sin^2\theta}} \right) - e^{-jk_{2z}2h}}{1 - \left(\frac{\cos\theta - \sqrt{\varepsilon_r - \sin^2\theta}}{\cos\theta + \sqrt{\varepsilon_r - \sin^2\theta}} \right) e^{-jk_{2z}2h}} \right) \right),
\end{aligned}
\tag{10}
$$

$$
f_z = -\frac{\cos\gamma \sin\theta}{\varepsilon_r} \left(\frac{1 + \left(\frac{\varepsilon_r \cos\theta - \sqrt{\varepsilon_r - \sin^2\theta}}{\varepsilon_r \cos\theta + \sqrt{\varepsilon_r - \sin^2\theta}} \right)}{1 + \left(\frac{\varepsilon_r \cos\theta - \sqrt{\varepsilon_r - \sin^2\theta}}{\varepsilon_r \cos\theta + \sqrt{\varepsilon_r - \sin^2\theta}} \right) e^{-jk_{2z}2h}} \right). \tag{11}
$$

By replacing (x_1, y_1), (x_2, y_2) by (x_5, y_5), (x_6, y_6) or (x_3, y_3), (x_4, y_4) by (x_7, y_7), (x_8, y_8), the expressions similar to (6) or (7) may also be used to calculate the equivalent sources (V_c, I_c) or (V_d, I_d) induced at the terminal of c- or d-arms merely. In (1)–(11) (μ_0, ε_0) are the permeability and permittivity of free space, respectively, ε_r is the relative permittivity of microstrip substrate.

Similar expressions to the equivalent source expressions (6) or (7) formulated for the a- or b-arms of the cross bend (Fig. 1), with suitable modification, may also be employed to discuss other typical discontinuous microstrip structures containing a right-angle bend and a T-type bend, observed in complicated microstrip circuits.

In this study, a fast model for radiated susceptibility problems associated with the microstrip circuits is proposed. Specifically, the key simulation processes include three steps:

1) The field-induced equivalent sources (V_a, I_a), (V_b, I_b), (V_c, I_c) or (V_d, I_d) along each microstrip element, such as the a-, b-, c-, or d-arms in Fig. 1, are calculated by substituting the parameters into (6) or (7), which associated with the location (x_i, y_i), the microstrip $(\varepsilon_r, h, w, l_i, d_i)$, and the incident plane wave $(E_0, \gamma, \theta, \phi)$.

2) The field-induced equivalent sources for each microstrip element are calculated by Matlab, and incorporated into a commercial circuit solver ADS. Thereafter the proposed fast model is established which includes the effects of EMI.

3) The excitation sources are added to the equivalent circuit obtained in step two, so that one may use ADS to simulate the output terminal voltage and current of the whole circuit. The susceptibility characteristics of the whole circuit are also analyzed.

The proposed fast model based on the equivalent expressions (6) and (7), which may be calculated by Matlab, and ADS will be used to solve the passive and active microstrip circuits, such as a cross bend, a single-stage amplifier and a band-rejection filter, which all contain discontinuous microstrip elements. Apparently, most of the microstrip elements for impedance matching and interconnection are almost along x and y-directions in microstrip circuits. Thus, the expressions (6) and (7) would be useful for characterizing the electromagnetism susceptibility problems of microstrip circuits.

3. SIMULATION RESULTS

In this section, three examples are presented to demonstrate the validity and accuracy of the model developed in this paper. In order to verify the accuracy of the proposed fast model based on the field-induced equivalent source expressions (6) and (7), a cross bend example is simulated and the results are compared with that from measurement. Specifically, the field-induced responses of discontinuous microstrip circuits (such as amplifiers and filers) will be discussed under the CW/pulse source excitation schemes.

3.1. Microstrip Cross Bend

The microstrip cross bend on the FR4 substrate, as shown in Fig. 1, is firstly examined for demonstration by using the equivalent source expressions and ADS circuit solver. Here, the coupling between elements is neglected, so that the cross bend is modeled as a cascade of four single microstrip elements with a cross-bend junction. The substrate and microstrip are characterized by $\varepsilon_r = 4.6$, $h = 1.6\,\text{mm}$, $w = 5\,\text{mm}$ and $l_1 = l_2 = d_1 = d_2 = 5\,\text{cm}$. Each trace is connected to the 50-Ω load at the termination. The cross bend is illuminated by a plane wave with an electric-field amplitude of $E_0 = 3\,\text{V/m}$, over the frequency range 300 MHz–4 GHz. The incident plane wave illuminates the structure from a direction $\theta = \phi = 0°$ with a $\gamma = 0°$ polarized electric field. The results measured in [23] are also included for comparison.

Figure 3 shows the field-induced voltage responses across the output terminal (x_6, y_6) of the microstrip cross bend. It shows a better agreement between the results obtained from this model and the measurement, than those obtained from [23] and measurement, especially in the high-frequency region. The better results, which are achieved by this paper than that by [23], are owing to a more accurate equivalent circuit of the cross-bend junction. Obviously, the method described above is validated to be useful and accurate.
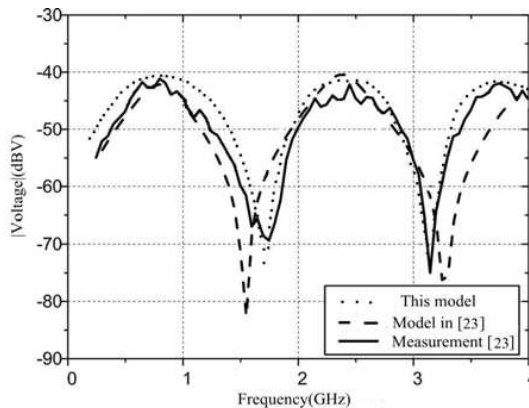
Figure 3. Measurement and simulation results for the field-induced output terminal voltages of the microstrip cross-bend structure, which is illuminated by an electric field of amplitude $E_0 = 3\,\text{V/m}$, $\gamma = \theta = \phi = 0°$.

3.2. Microstrip Band-rejection Filter

A microstrip band-rejection filter is simulated in this example to verify the accuracy of the proposed method where the configuration of the microstrip filter is taken from [24] and repeated here in Fig. 4. The substrate is characterized by $\varepsilon_r = 10$ and $h = 0.635\,\text{mm}$. The S-parameters associated with this filter are depicted in Fig. 5.

The transient simulation results, which are obtained by the proposed method in this paper and the coupled FDTD macromodeling and circuit simulation approach presented by [25], are shown in Fig. 6, which characterize the transient output responses of the filter circuit. The good agreements between the results of the method described above and that of the integrated approach verify the validity and accuracy of the proposed method.

Note that the proposed model has the merit of very short simulation time. For instance, the total CPU time taken by the transient simulation of this example is only less than 10 seconds in comparison to more than 2 minutes consumed by using macromodeling and circuit simulation approach on a PC.
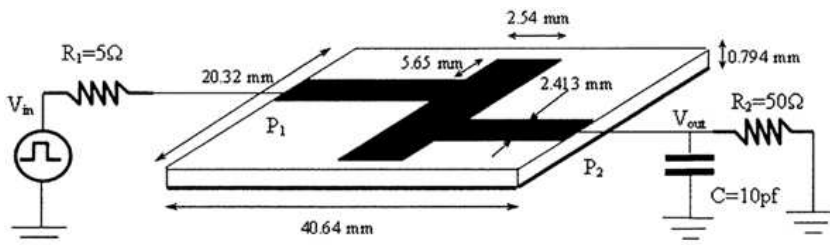
Figure 4. Circuit schematic of a microstrip band-rejection filter.
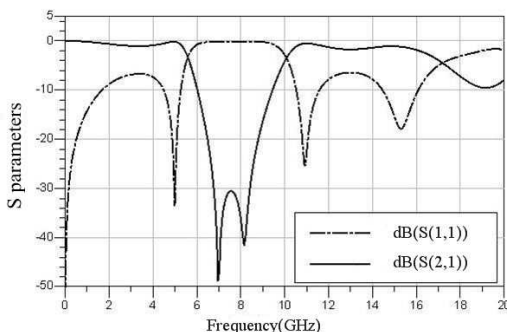
Figure 5. S parameters of the microstrip band-rejection filter.
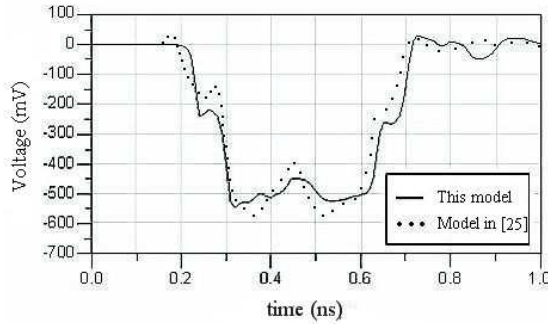
Figure 6. Transient simulation results for the field-induced output terminal voltages of the band-rejection filter, which is illuminated by an electric-field amplitude of $E_0 = 500 \, \text{V/m}$, $\gamma = \theta = \phi = 90°$.

(a)   (b)
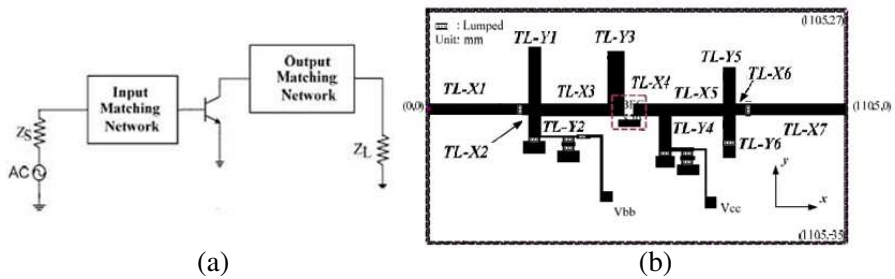
Figure 7. Single-stage microstrip amplifier, (a) schematic diagram, (b) layout with transistor (BFG 520) and lumped elements removed.

3.3. Single-stage Amplifier

The single-stage amplifier shown in Fig. 7 is analyzed by using the proposed method in this paper to discuss the radiated susceptibility problem. The amplifier which is from [26] under consideration is implemented in PCB on the FR4 substrate. It consists of the BFG520 transistor, input and output impedance matching networks, and other necessary circuits on the PCB with routing, as shown in Fig. 7. This single-stage amplifier may be regarded as a cascade of many single microstrip elements with bends to deal with the EM compatibility problems.

The layout of this single-stage amplifier (operated at 1.7 GHz), with transistors and lumped elements removed, is illustrated in Fig. 7(b). The length and width of each microstrip interconnect

Table 1. Geometric parameters for microstrip line elements in Fig. 7(b).

Element	Width (mm)	Started point (mm)	Terminated point (mm)
TL-X1	3.16	(0, 0)	(24, 0)
TL-X2	3.16	(25, 0)	(28, 0)
TL-X3	3.16	(30, 0)	(48, 0)
TL-X4	3.16	(55, 0)	(62, 0)
TL-X5	3.16	(70, 0)	(84, 0)
TL-X6	3.16	(82, 0)	(85, 0)
TL-X7	3.16	(86, 0)	(111.5, 0)
TL-Y1	3.16	(29,1.6)	(29,16.6)
TL-Y2	3.16	(29, −1.6)	(29, −7.6)
TL-Y3	4.5	(50, 1.6)	(50, 15.6)
TL-Y4	3.16	(67, −1.6)	(67, −10.4)
TL-Y5	3.16	(80, 1.6)	(80, 11.1)
TL-Y6	3.16	(80, −1.6)	(80, −8.7)

are properly designed to meet the amplifier impedance matching conditions, and the corresponding values are given in Table 1. For the purpose of simulation and fabrication, the length of each microstrip interconnect element is extracted by the ADS circuit solver, and the corresponding location parameters in rectangular coordinate system which are designed to meet amplifier impedance matching conditions, are given in Table 1.

The single-stage amplifier, implemented on the FR4 substrate ($\varepsilon_r = 4.6$, $h = 1.6$ mm), presents a gain of 10 dB, as given in [26]. This transistor amplifier circuit is excited by CW sources of −10 dB and −20 dB, with a frequency 1.7 GHz, and the output is connected to the 50-Ω loads. The study is performed for a low power interference. This amplifier is illuminated by a plane wave with $E_0 = 3$ V/m and $\gamma = \theta = \phi = 0°$, over the frequency range 800 MHz–4 GHz, and its dc bias voltages are provided by the batteries for which $V_{cc} = 3$ V and $V_{bb} = 1$ V (Fig. 7).

The simulation results are compared with the measurement results obtained by [26] in Fig. 8, which characterize the field-induced output

(a)   (b)
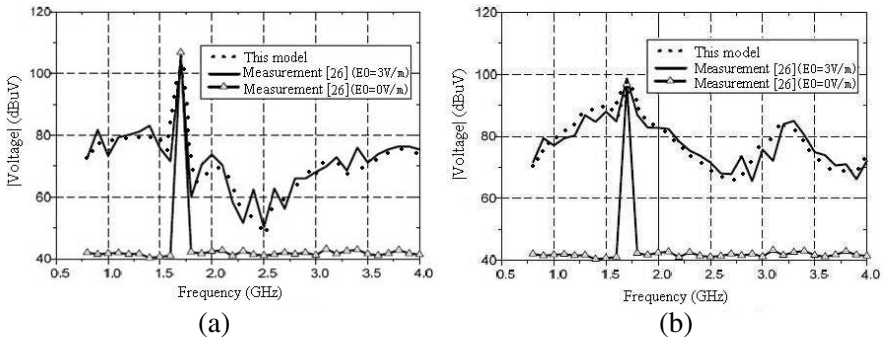
Figure 8. Measurement and simulation results for the field-induced output terminal voltages of the single-stage amplifier, which is excited by a CW source and is illuminated by an electric-field amplitude of $E_0 = 3$ or 0 V/m. (a) A CW source of -10 dBm, $\gamma = \theta = 0°$, $\phi = 90°$, (b) a CW source of -20 dBm, $\gamma = \theta = \phi = 0°$.

voltages at the terminal of the amplifier under CW excitation and illuminated by the plane wave. As shown, there is a good agreement among the simulation and measurement results. The measurement results with the absence of the incident wave ($E_0 = 0$ V/m) are also presented for comparison. Especially, we may conclude that the incident plane wave will influence the output terminal responses significantly. The proposed fast model is validated again to be very efficient in analyzing the important radiated susceptibility problems associated with the active and passive microstrip circuits, containing the interconnect discontinuities on the PCB.

4. CONCLUSION

A fast model, based on the equivalent source expressions and the circuit solver, has been proposed to analyze the electromagnetic susceptibility problems of the microstrip circuits, especially the discontinuous microstrip interconnect structures are considered in the cases. The microstrip circuits, such as the cross bend, the band-rejection filter and the single-stage amplifier, are simulated to validate the accuracy of the proposed method. Results obtained by these models agree well with those from other methods. In addition, one can calculate the output responses faster using this method than traditional methods. With the merit of short simulation time, the proposed model would be very useful and efficient for the analysis of the electromagnetic susceptibility problems, typically for the discontinuous microstrip circuits.

ACKNOWLEDGMENT

REFERENCES

1. Ramdani, M., E. Sicard, A. Boyer, S. Ben Dhia, J. J. Whalen, T. H. Hubing, M. Coenen, and O. Wada, "The electromagnetic compatibility of integrated circuits — Past, present, and future," *IEEE Trans. on Electromagn. Compat.*, Vol. 51, No. 1, 78–100, 2009.

2. Du, Y. and B. Liu, "A numerical method for electromagnetic scattering from dielectric rough surfaces based on the stochastic second degree method," *Progress In Electromagnetics Research*, Vol. 97, 327–342, 2009.

3. Soproni, V. D., S. M. Vicas, T. Leuca, M. N. Arion, F. I. Hathazi, and C. O. Molnar, "High frequency electromagnetic field modeling and experimental validation of the microwave drying of wheat seeds," *Progress In Electromagnetics Research B*, Vol. 41, 419–439, 2012.

4. Lagos, J. L. and F. Fiori, "Worst-case induced disturbances in digital and analog interchip interconnects by an external electromagnetic plane wave — Part I: Modeling and algorithm," *IEEE Trans. on Electromagn. Compat.*, Vol. 53, No. 1, 178–184, 2011.

5. Tsai, H. C., "Investigation into time-and-frequency-domain EMI-induced noise in bistable multi-vibrator," *Progress In Electromagnetics Research*, Vol. 100, 327–349, 2010.

6. Han, S. M., J.-J. Bang, C.-S. Huh, and J.-S. Choi, "A PCB noise analysis regarding EMP penetration using an electromagnetic topology method," *Progress In Electromagnetics Research*, Vol. 122, 15–27, 2012.

7. Xie, H., J. Wang, R. Fan, and Y. Liu, "Spice models for radiated and conducted susceptibility analyses of multiconductor shielded cables," *Progress In Electromagnetics Research*, Vol. 103, 241–257, 2010.

8. Rachidi, F., "Formulation of the field-to-transmission line coupling equations in terms of magnetic excitation field," *IEEE Trans. on Electromagn. Compat.*, Vol. 35, No. 3, 404–407, 1993.

9. Bernardi, P. and R. Cicchetti, "Response of a planar microstrip line excited by an external electromagnetic field," *IEEE Trans. on Electromagn. Compat.*, Vol. 32, No. 2, 98–105, 1990.

10. Tesche, F. M., M. V. Ianoz, and T. Karlsson, *EMC Analysis Methods and Computational Models*, Wiley, New York, 1997.

11. Khazaka, R. and M. Nakhla, "Analysis of high-speed interconnects in the presence of electromagnetic interference," *IEEE Trans. on Micro. Theory and Tech.*, Vol. 46, No. 7, 940–947, 1998.

12. Liu, E. X., E. P. Li, L. W. Li, and Z. Shen, "Finite-difference time-domain macromodel for simulation of electromagnetic interference at high-speed interconnects," *IEEE Trans. on Magn.*, Vol. 41, No. 1, 65–71, 2005.

13. Taylor, C. D., R. S. Satterwhite, and C. W. Harrison, "The response of a terminated two-wire transmission line excited by a nonuniform electromagnetic field," *IEEE Trans. on Antennas and Propag.*, Vol. 13, No. 6, 987–989, 1965.

14. Taflove, A. and S. C. Hagness, *Computational Electrodynamics: The Finite-difference Time-domain Method*, Artech House, Boston, 2000.

15. Silva, A. O., R. Bertholdo, M. G. Schiavetto, B.-H. V. Borges, S. J. L. Ribeiro, Y. Messaddeq, and M. A. Romero, "Comparative analysis between experimental characterization results and numerical FDTD modelling of self-assembled photonic crystals," *Progress In Electromagnetics Research B*, Vol. 23, 329–342, 2010.

16. Lan, J., Y. Yang, and J. Y. Dai, "Applications of a three-dimensional FDTD method with weakly conditional stability to the analysis of microstrip filters with fine scale structures," *Progress In Electromagnetics Research Letters*, Vol. 27, 101–115, 2011.

17. Dzulkipli, I., M. H. Jamaluddin, R. Ngah, M. R. B. Kamarudin, N. Seman, and M. K. A. Rahim, "Mutual coupling analysis using FDTD for dielectric resonator antenna reflectarray radiation prediction," *Progress In Electromagnetics Research B*, Vol. 41, 121–136, 2012.

18. Wang, J., W.-Y. Yin, J.-P. Fang, and Q.-F. Liu, "Transient responses of coaxial cables in an electrically large cabin with slots and windows illuminated by an electromagnetic pulse," *Progress In Electromagnetics Research*, Vol. 106, 1–16, 2010.

19. Xie, H. Y., J. G. Wang, and R. Y. Fan, "A hybrid FDTD-SPICE method for transmission lines excited by a nonuniform incident Wave," *IEEE Trans. on Electromagn. Compat.*, Vol. 51, No. 3, 811–817, 2009.

20. Cheldavi, A. and P. Nayeri, "Analysis of V transmission lines response to external electromagnetic fields," *Progress In Electromagnetics Research*, Vol. 68, 297–315, 2007.

21. Gupta, K. C., R. Garg, I. Bahl, and P. Bhartia, *Microstrip Line and Slotlines.*, 2nd Edition, Artech House, Boston, 1996.

22. Leone, M. and H. L. Singer, "On the coupling of an external electromagnetic field to a printed circuit board trace," *IEEE Trans. on Electromagn. Compat.*, Vol. 41, No. 4, 418–424, 1999.

23. Hsieh, H. C., C. N. Chiu, M. S. Lin, C. H. Wang, and C. H. Chen, "An equation-based hybrid method for predicting radiated susceptibility responses of RF/Microwave circuits," *IEEE Trans. on Electromagn. Compat.*, Vol. 53, No. 2, 339–348, 2011.

24. Li, E. P., E. X. Liu, L. W. Li, and M. S. Leong, "A coupled efficient and systematic full-wave time-domain macromodeling and circuit simulation," *IEEE Transactions on Advanced Packaging*, Vol. 27, No. 1, 1–11, 2004.

25. Jin, H. F., E. P. Li, and E. X. Liu, "A novel integrated approach for simulation of electromagnetic susceptibility problem," *2005 International Symposium on Electromagnetic Compatibility*, Vol. 2, 446–450, 2005.

26. Hsieh, H.-C., J. S. Chen, C.-H. Wang, C.-N. Chiu, M.-S. Lin, and C. H. Chen, "A fast analysis of electromagnetic immunity responses of RF amplifier circuit under CW/digital-modulation schemes," *2011 IEEE International Symposium on Electromagnetic Compatibility (EMC)*, 724–728, 2011.